Eur. Phys. J. C 22, 613–626 (2002)
Digital Object Identifier (DOI) 10.1007/s100520100851

THE EUROPEAN PHYSICAL JOURNAL C

Inclusive semileptonic branching ratios of b hadrons produced in Z decays

The ALEPH Collaboration

A. Heister, S. Schael
Physikalisches Institut das RWTH-Aachen, 52056 Aachen, Germany

R. Barate, I. De Bonis, D. Decamp, C. Goy, J.-P. Lees, E. Merle, M.-N. Minard, B. Pietrzyk
Laboratoire de Physique des Particules (LAPP), IN^2P^3-CNRS, 74019 Annecy-le-Vieux Cedex, France

S. Bravo, M.P. Casado, M. Chmeissani, J.M. Crespo, E. Fernandez, M. Fernandez-Bosman, Ll. Garrido[15], E. Graugés, M. Martinez, G. Merino, R. Miquel[27], Ll.M. Mir[27], A. Pacheco, H. Ruiz
Institut de Fśica d'Altes Energies, Universitat Autònoma de Barcelona, 08193 Bellaterra (Barcelona), Spain[7]

A. Colaleo, D. Creanza, M. de Palma, G. Iaselli, G. Maggi, M. Maggi, S. Nuzzo, A. Ranieri, G. Raso[23], F. Ruggieri, G. Selvaggi, L. Silvestris, P. Tempesta, A. Tricomi[3], G. Zito
Dipartimento di Fisica, INFN Sezione di Bari, 70126 Bari, Italy

X. Huang, J. Lin, Q. Ouyang, T. Wang, Y. Xie, R. Xu, S. Xue, J. Zhang, L. Zhang, W. Zhao
Institute of High Energy Physics, Academia Sinica, Beijing, P.R. China[8]

D. Abbaneo, P. Azzurri, G. Boix[6], O. Buchmüller, M. Cattaneo, F. Cerutti, B. Clerbaux, G. Dissertori, H. Drevermann, R.W. Forty, M. Frank, T.C. Greening[29], J.B. Hansen, J. Harvey, P. Janot, B. Jost, M. Kado, P. Mato, A. Moutoussi, F. Ranjard, L. Rolandi, D. Schlatter, O. Schneider[2], W. Tejessy, F. Teubert, E. Tournefier[25], J. Ward
European Laboratory for Particle Physics (CERN), 1211 Geneva 23, Switzerland

Z. Ajaltouni, F. Badaud, A. Falvard[22], P. Gay, P. Henrard, J. Jousset, B. Michel, S. Monteil, J-C. Montret, D. Pallin, P. Perret, F. Podlyski
Laboratoire de Physique Corpusculaire, Université Blaise Pascal, IN^2P^3-CNRS, Clermont-Ferrand, 63177 Aubière, France

J.D. Hansen, J.R. Hansen, P.H. Hansen, B.S. Nilsson, A. Wäänänen
Niels Bohr Institute, 2100 Copenhagen, Denmark[9]

A. Kyriakis, C. Markou, E. Simopoulou, A. Vayaki, K. Zachariadou
Nuclear Research Center Demokritos (NRCD), 15310 Attiki, Greece

A. Blondel[12], G. Bonneaud, J.-C. Brient, A. Rougé, M. Rumpf, M. Swynghedauw, M. Verderi, H. Videau
Laboratoire de Physique Nucléaire et des Hautes Energies, Ecole Polytechnique, IN^2P^3-CNRS, 91128 Palaiseau Cedex, France

V. Ciulli, E. Focardi, G. Parrini
Dipartimento di Fisica, Università di Firenze, INFN Sezione di Firenze, 50125 Firenze, Italy

A. Antonelli, M. Antonelli, G. Bencivenni, G. Bologna[4], F. Bossi, P. Campana, G. Capon, V. Chiarella, P. Laurelli, G. Mannocchi[5], F. Murtas, G.P. Murtas, L. Passalacqua, M. Pepe-Altarelli[24], P. Spagnolo
Laboratori Nazionali dell'INFN (LNF-INFN), 00044 Frascati, Italy

A.W. Halley, J.G. Lynch, P. Negus, V. O'Shea, C. Raine, A.S. Thompson
Department of Physics and Astronomy, University of Glasgow, Glasgow G12 8QQ, UK[10]

S. Wasserbaech
Department of Physics, Haverford College, Haverford, PA 19041-1392, USA

R. Cavanaugh, S. Dhamotharan, C. Geweniger, P. Hanke, G. Hansper, V. Hepp, E.E. Kluge, A. Putzer, J. Sommer, K. Tittel, S. Werner[19], M. Wunsch[19]
Kirchhoff-Institut für Physik, Universität Heidelberg, 69120 Heidelberg, Germany[16]

R. Beuselinck, D.M. Binnie, W. Cameron, P.J. Dornan, M. Girone[1], N. Marinelli, J.K. Sedgbeer, J.C. Thompson[14]
Department of Physics, Imperial College, London SW7 2BZ, UK[10]

V.M. Ghete, P. Girtler, E. Kneringer, D. Kuhn, G. Rudolph
Institut für Experimentalphysik, Universität Innsbruck, 6020 Innsbruck, Austria[18]

E. Bouhova-Thacker, C.K. Bowdery, A.J. Finch, F. Foster, G. Hughes, R.W.L. Jones[1], M.R. Pearson, N.A. Robertson
Department of Physics, University of Lancaster, Lancaster LA1 4YB, UK[10]

I. Giehl, K. Jakobs, K. Kleinknecht, G. Quast, B. Renk, E. Rohne, H.-G. Sander, H. Wachsmuth, C. Zeitnitz
Institut für Physik, Universität Mainz, 55099 Mainz, Germany[16]

A. Bonissent, J. Carr, P. Coyle, O. Leroy, P. Payre, D. Rousseau, M. Talby
Centre de Physique des Particules, Université de la Méditerranée, IN^{2}P^3-CNRS, 13288 Marseille, France

M. Aleppo, F. Ragusa
Dipartimento di Fisica, Università di Milano e INFN Sezione di Milano, 20133 Milano, Italy

A. David, H. Dietl, G. Ganis[26], K. Hüttmann, G. Lütjens, C. Mannert, W. Männer, H.-G. Moser, R. Settles, H. Stenzel, W. Wiedenmann, G. Wolf
Max-Planck-Institut für Physik, Werner-Heisenberg-Institut, 80805 München, Germany[p]

J. Boucrot, O. Callot, M. Davier, L. Duflot, J.-F. Grivaz, Ph. Heusse, A. Jacholkowska[22], J. Lefrançois, J.-J. Veillet, I. Videau, C. Yuan
Laboratoire de l'Accélérateur Linéaire, Université de Paris-Sud, IN^{2}P^3-CNRS, 91898 Orsay Cedex, France

G. Bagliesi, T. Boccali, L. Foà, A. Giammanco, A. Giassi, F. Ligabue, A. Messineo, F. Palla, G. Sanguinetti, A. Sciabà, G. Sguazzoni, R. Tenchini[1], A. Venturi, P.G. Verdini
Dipartimento di Fisica dell'Università, INFN Sezione di Pisa, e Scuola Normale Superiore, 56010 Pisa, Italy

G.A. Blair, G. Cowan, M.G. Green, T. Medcalf, A. Misiejuk, J.A. Strong, P. Teixeira-Dias, J.H. von Wimmersperg-Toeller
Department of Physics, Royal Holloway & Bedford New College, University of London, Egham, Surrey TW20 OEX, UK[10]

R.W. Clifft, T.R. Edgecock, P.R. Norton, I.R. Tomalin
Particle Physics Dept., Rutherford Appleton Laboratory, Chilton, Didcot, Oxon OX11 OQX, UK[10]

B. Bloch-Devaux[1], P. Colas, S. Emery, W. Kozanecki, E. Lançon, M.-C. Lemaire, E. Locci, P. Perez, J. Rander, J.-F. Renardy, A. Roussarie, J.-P. Schuller, J. Schwindling, A. Trabelsi[21], B. Vallage
CEA, DAPNIA/Service de Physique des Particules, CE-Saclay, 91191 Gif-sur-Yvette Cedex, France[17]

N. Konstantinidis, A.M. Litke, G. Taylor
Institute for Particle Physics, University of California at Santa Cruz, Santa Cruz, CA 95064, USA[13]

C.N. Booth, S. Cartwright, F. Combley[4], M. Lehto, L.F. Thompson
Department of Physics, University of Sheffield, Sheffield S3 7RH, UK[10]

K. Affholderbach[28], A. Böhrer, S. Brandt, C. Grupen, A. Ngac, G. Prange, U. Sieler
Fachbereich Physik, Universität Siegen, 57068 Siegen, Germany[16]

G. Giannini
Dipartimento di Fisica, Università di Trieste e INFN Sezione di Trieste, 34127 Trieste, Italy

J. Rothberg
Experimental Elementary Particle Physics, University of Washington, Seattle, WA 98195, USA

S.R. Armstrong, K. Cranmer, P. Elmer, D.P.S. Ferguson, Y. Gao[20], S. González, O.J. Hayes, H. Hu, S. Jin, J. Kile, P.A. McNamara III, J. Nielsen, W. Orejudos, Y.B. Pan, Y. Saadi, I.J. Scott, J. Walsh, Sau Lan Wu, X. Wu, G. Zobernig
Department of Physics, University of Wisconsin, Madison, WI 53706, USA[11]

Received: 1 August 2001 /
Published online: 14 December 2001 – © Springer-Verlag / Società Italiana di Fisica 2001

Abstract. A measurement of the inclusive semileptonic branching ratios of b hadrons produced in Z decay is presented, using four million hadronic events collected by the ALEPH detector from 1991 to 1995. Electrons and muons are selected opposite to b-tagged hemispheres. Two different methods are explored to distinguish the contributions from direct $b \to X\ell\nu$ and cascade $b \to c \to X\ell\nu$ decays to the total lepton

yield. One is based on the lepton transverse momentum spectrum, the other makes use of the correlation between the charge of the lepton and charge estimators built from tracks in the opposite hemisphere of the event. The latter method reduces the dependence on the modelling of semileptonic b decays. The results obtained by averaging the two techniques are

$$\mathrm{BR}(\mathrm{b} \to \mathrm{X}\ell\nu) = 0.1070 \pm 0.0010_{\,\mathrm{stat}} \pm 0.0023_{\,\mathrm{syst}} \pm 0.0026_{\,\mathrm{model}} ,$$
$$\mathrm{BR}(\mathrm{b} \to \mathrm{c} \to \mathrm{X}\ell\nu) = 0.0818 \pm 0.0015_{\,\mathrm{stat}} \pm 0.0022_{\,\mathrm{syst}} \,^{+0.0010}_{-0.0014\,\mathrm{model}} .$$

1 Introduction

Accurate knowledge of the direct inclusive semileptonic branching fraction of b hadrons, $\mathrm{BR}(\mathrm{b} \to \mathrm{X}\ell\nu)$ (ℓ = e or μ), provides the opportunity to test and improve the theoretical models describing the dynamics of heavy hadrons. It is also an important input to a determination of $|V_{\mathrm{cb}}|$ [1,2]. Together with the cascade decay branching fraction $\mathrm{BR}(\mathrm{b} \to \mathrm{c} \to \mathrm{X}\ell\nu)$, $\mathrm{BR}(\mathrm{b} \to \mathrm{X}\ell\nu)$ is an important input parameter for many heavy flavour analyses.

Previous determinations of $\mathrm{BR}(\mathrm{b} \to \mathrm{X}\ell\nu)$ performed at the Z and the $\Upsilon(4\mathrm{S})$ have shown some disagreement, with that measured at the Z being higher while the opposite would be expected from the short b baryon lifetime [3]. On the other hand, theoretical predictions have tended to be higher than experimental measurements although recent calculations, including higher order perturbative QCD corrections, give values in better agreement [4,5].

In this paper two new analyses are presented, based on the data collected with the ALEPH detector from 1991 to 1995. Two different methods are used to distinguish the contributions from the direct and cascade decays to the total lepton yield. One method has better statistical precision but a stronger dependence on the modelling of the semileptonic decays. The other is designed to have minimal decay modelling dependence. The efficiency of lepton identification is measured from data using several control samples. The description of the fragmentation of b quarks into b hadrons is based on the spectrum reconstructed with the ALEPH data [6] and is therefore independent of modelling assumptions.

2 The ALEPH detector

A detailed description of the ALEPH detector can be found in [7] and of its performance in [8]. A brief overview will be given here, along with some basic information about lepton identification.

Charged particles are detected in the central part of the apparatus which consists of a high resolution silicon vertex detector (VDET), a cylindrical drift chamber (ITC) and a large time projection chamber (TPC).

The three tracking devices are immersed in a 1.5 T axial magnetic field provided by a superconducting solenoid; the particle momentum transverse to the beam axis is measured with a resolution $\sigma(p_{\mathrm{T}})/p_{\mathrm{T}} = 6 \times 10^{-4} p_{\mathrm{T}} \oplus 5 \times 10^{-3}$, with p_{T} measured in GeV/c. In the following, charged tracks are defined as "good" if a) they originate from within a cylinder, coaxial with the beam and centred around the nominal interaction point, with length 20 cm and radius 2 cm; b) their polar angle with respect to the beam satisfies the requirement $|\cos\theta| < 0.95$; and c) at least four hits are reconstructed in the TPC.

[1] Also at CERN, 1211 Geneva 23, Switzerland
[2] Now at Université de Lausanne, 1015 Lausanne, Switzerland
[3] Also at Dipartimento di Fisica di Catania and INFN Sezione di Catania, 95129 Catania, Italy
[4] Deceased
[5] Also Istituto di Cosmo-Geofisica del C.N.R., Torino, Italy
[6] Supported by the Commission of the European Communities, contract ERBFMBICT982894
[7] Supported by CICYT, Spain
[8] Supported by the National Science Foundation of China
[9] Supported by the Danish Natural Science Research Council
[10] Supported by the UK Particle Physics and Astronomy Research Council
[11] Supported by the US Department of Energy, grant DE-FG0295-ER40896
[12] Now at Departement de Physique Corpusculaire, Université de Genève, 1211 Genève 4, Switzerland
[13] Supported by the US Department of Energy, grant DE-FG03-92ER40689
[14] Also at Rutherford Appleton Laboratory, Chilton, Didcot, UK
[15] Permanent address: Universitat de Barcelona, 08208 Barcelona, Spain
[16] Supported by the Bundesministerium für Bildung, Wissenschaft, Forschung und Technologie, Germany
[17] Supported by the Direction des Sciences de la Matière, C.E.A
[18] Supported by the Austrian Ministry for Science and Transport
[19] Now at SAP AG, 69185 Walldorf, Germany
[20] Also at Department of Physics, Tsinghua University, Beijing, The People's Republic of China
[21] Now at Département de Physique, Faculté des Sciences de Tunis, 1060 Le Belvédère, Tunisia
[22] Now at Groupe d' Astroparticules de Montpellier, Université de Montpellier II, 34095 Montpellier, France
[23] Also at Dipartimento di Fisica e Tecnologie Relative, Università di Palermo, Palermo, Italy
[24] Now at CERN, 1211 Geneva 23, Switzerland
[25] Now at ISN, Institut des Sciences Nucléaires, 53 Av. des Martyrs, 38026 Grenoble, France
[26] Now at INFN Sezione di Roma II, Dipartimento di Fisica, Universitá di Roma Tor Vergata, 00133 Roma, Italy
[27] Now at LBNL, Berkeley, CA 94720, USA
[28] Now at Skyguide, Swissair Navigation Services, Geneva, Switzerland
[29] now at Honeywell, Phoenix AZ, USA

Hemispheres containing b quarks are identified with a lifetime b-tagging algorithm [9] which exploits the three-dimensional impact parameter resolution of the charged tracks. For tracks with two space points in the VDET (*i.e.* $|\cos\theta| < 0.7$) the resolution can be parametrized as $(25 + 95/p)\,\mu$m, with p measured in GeV/c.

The TPC also provides up to 338 measurements of the specific ionization energy loss (dE/dx) which allows electrons to be separated from other charged particles by more than three standard deviations up to a momentum of 8 GeV/c.

Electrons are identified by the characteristic longitudinal and transverse development of their associated showers in the 22 radiation length electromagnetic calorimeter (ECAL). The ECAL is segmented in $0.9^\circ \times 0.9^\circ$ projective towers, read out in three longitudinal stacks; the energy resolution achieved for isolated electrons and photons is $\sigma_E/E = 0.009 + 0.18/\sqrt{E}$, with E measured in GeV. The dE/dx information provided by the TPC enhances the hadron rejection power, while non-prompt electrons originating from photon conversions in the material of the detector are rejected on the basis of their kinematic and geometric properties.

Muons are identified by their penetration pattern in the hadronic calorimeter (HCAL); the additional three-dimensional coordinates measured in two layers of external muon chambers help in resolving the remaining possible ambiguities.

The standard lepton identification technique is described in detail in [10]. For the analyses presented in this paper, the selection is improved and optimized to reduce the systematic uncertainty on the results, as discussed in Sect. 4.

3 Event samples

The analysis is based on nearly four million hadronic Z decays selected using charged track information [11]. This data set was reprocessed during 1998 using improved reconstruction algorithms. The main benefits for this analysis are related to the enhanced particle identification capabilities, and are discussed in the description of the lepton selection (Sect. 4).

The statistics available for the simulation are larger than the data statistics by a factor of two; an additional sample of about five million $Z \to b\bar{b}$ simulated events is used for the estimate of the correlation between the b-tagging probability and the lepton selection efficiency (Sect. 6.14). Each event is divided into two hemispheres by the plane perpendicular to the thrust axis. Three samples of lepton candidates are selected as follows.

Sample $\mathcal{B}$. A b-tagging variable $\mathcal{B}_{\rm tag}$, based on the large mass and lifetime of b hadrons, is built as in [9] (Fig. 1). This variable is defined using tracks contained in one hemisphere, but here the primary vertex is reconstructed using all tracks of the events, in contrast with [9]. The impact parameter in the simulation has been smeared in order to reproduce the resolution measured in the data, following the same procedure as in [9]. The algorithm has good performance for events well contained in the vertex detector acceptance; events with $|\cos\theta_{\rm thrust}| > 0.7$ are rejected.

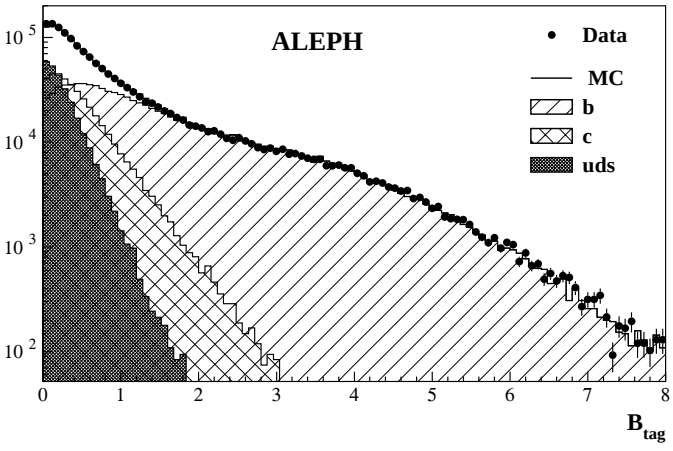

Fig. 1. Distribution of the b-tagging variable built by combining both lifetime and mass information of tracks in each hemisphere opposite to a lepton candidate. The error bars show the statistical error in the data only

A cut $\mathcal{B}_{\rm tag} > 2$ is applied, selecting 345,555 hemispheres in the data, with a b purity of 97%. The cut is about 32% efficient on b hemispheres within the angular region considered.

Lepton candidates (electron or muon) are searched for in hemispheres opposite to the selected ones. Events in which both hemispheres are b-tagged are used twice. The candidates are ordered according to their transverse momentum $p_\perp$, measured with respect to the jet axis with the lepton excluded from the jet as in [10]. When more than one lepton is found in a given hemisphere, the two leptons with highest $p_\perp$ and with opposite-charge are used for the analysis; if all have the same charge the one with the highest $p_\perp$ is taken. A total of 80,730 lepton candidates are finally selected.

Sample $\mathcal{P}$. In each event one of the two hemispheres is randomly chosen, and a lepton candidate fulfilling the requirement $p_\perp > 1.25$ GeV/c is searched for. This selects 148,001 hemispheres in the data with an estimated b purity of 90% and a b efficiency of 12%. Since the $p_\perp$ cut suppresses cascade decays, the charge Q of the lepton is a good estimator of the charge of the quark at production time, leading to a probability of tagging the charge correctly of $P^{\mathcal{P}}_{\rm b\bar{b}} = 0.81 \pm 0.01$; this includes the dilution due to neutral B meson mixing. This value is measured from the data with the method described later in Sect. 5.4, and is in good agreement with the prediction of the simulation, $P^{\mathcal{P}}_{\rm b\bar{b}}({\rm MC}) = 0.817 \pm 0.004_{\rm stat}$. As this selection does not rely specifically on the vertex detector, no cut is made on $|\cos\theta_{\rm thrust}|$. The distribution of $Q \times p_\perp$ is shown in Fig. 2.

Leptons are searched for in hemispheres opposite to the tagged ones, as in the case of the $\mathcal{B}$ sample, yielding a total of 14,509 candidates.

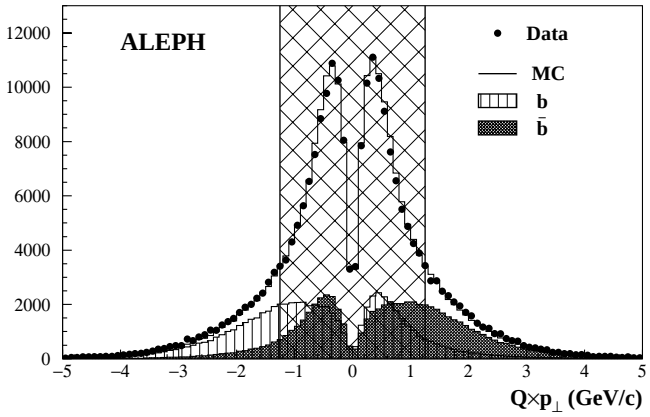

Fig. 2. The charge estimator $Q \times p_\perp$, based on the charge of a high $p_\perp$ lepton: data are compared with Monte Carlo simulation. The contributions of hemispheres containing b and $\overline{\mathrm{b}}$ quarks extracted from Monte Carlo are also shown. The cross-hatched area indicates the region rejected by the selection cut

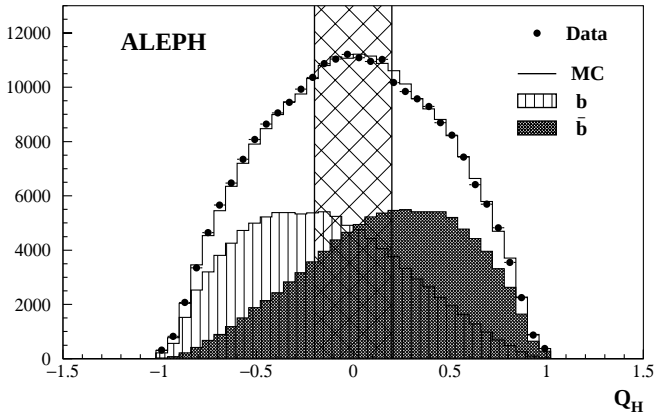

Fig. 3. Distribution of the hemisphere charge estimator Q_H, in data and simulation. The contributions of hemispheres containing b and $\overline{\mathrm{b}}$ quarks extracted from Monte Carlo are also shown. The cross-hatched area indicates the region rejected by the selection cut

The *a priori* random choice of the hemisphere used for charge tagging ensures that there is no double counting of lepton pairs, and allows the measurement of $P^{\mathcal{P}}_{\mathrm{b\bar{b}}}$ from the data (Sect. 5.4).

Sample $\mathcal{J}$. Two hemisphere charge estimators are calculated:

$$Q_p = \frac{\sum q\, p_\parallel^{\kappa_p}}{\sum p_\parallel^{\kappa_p}} \ , \qquad Q_s = \frac{\sum q\, s^{\kappa_s}}{\sum s^{\kappa_s}} \ ,$$

where the sum runs over all the good charged tracks, as defined in Sect. 2, with momentum in excess of 200 MeV/c, q is the charge, $p_\parallel$ the component of the momentum parallel to the thrust axis, s is the impact parameter significance, defined as in [9], $\kappa_p = 0.5$ and $\kappa_s = 0.3$. Tracks with negative impact parameter are not included in the definition of Q_s.

The two charge estimators are combined using weights w, parametrised as a function of their magnitudes to achieve optimal performance on b hemispheres:

$$Q_H = w(|Q_p|, |Q_s|)\, Q_p + [1 - w(|Q_p|, |Q_s|)]\, Q_s \ .$$

Hemispheres are selected if they satisfy $\mathcal{B}_{\mathrm{tag}} > 1.2$, which enhances the b content of the sample. In addition a cut $|Q_H| > 0.2$ is applied to ensure a good probability that the sign of Q_H is correlated with the charge of the b quark in the parent b hadron. The distribution of the Q_H variable is shown in Fig. 3, together with the contributions of hemispheres containing b and $\overline{\mathrm{b}}$ quarks. Since the $\mathcal{B}_{\mathrm{tag}}$ variable is used, events with $|\cos\theta_{\mathrm{thrust}}| > 0.7$ are not considered. Hemispheres containing a lepton candidate with $p_\perp > 1.25$ GeV/c are rejected in order to keep this sample statistically independent of sample $\mathcal{P}$.

The procedure selects 392,523 hemispheres in the data with an estimated b purity of 87% and a b efficiency of 32%. The probability of correct b charge tagging measured from the data is $P^{\mathcal{J}}_{\mathrm{b\bar{b}}} = 0.724 \pm 0.007$, again in good agreement with the Monte Carlo prediction $P^{\mathcal{J}}_{\mathrm{b\bar{b}}}(\mathrm{MC}) = 0.721 \pm 0.001_{\mathrm{stat}}$.

The lepton yield in hemispheres opposite to the selected ones is studied as for the previous samples, giving a total of 61,012 candidates.

4 Lepton identification

A good control of the identification efficiency, as well as of the background in the selected sample, is crucial for this analysis. The identification of electrons and muons follows the lines of [10]. A reduced dependence on the description of the b fragmentation is achieved by extending the acceptance to lower momentum leptons.

The main change is, however, the use of a new estimator for the charged particle energy loss in the TPC. In the reprocessing of the LEP I data sample, information from the pulse height measured by the TPC pads has been used to build a new estimator similar to that from the wire measurements. The pad estimator is available for all tracks, while the wire estimator is calculated only for tracks that have a minimum number of isolated wire signals, which leads to an average inefficiency of about 15% in the hadronic environment.

The wires estimator is defined as

$$I_i^{\mathrm{w}} = \frac{I^{\mathrm{w}}_{\mathrm{meas}} - \langle I^{\mathrm{w}} \rangle_i}{\sigma_i^{\mathrm{w}}},$$

where $\langle I^{\mathrm{w}} \rangle_i$ is the average energy loss expected for particle type i, σ_i^{w} is the expected width, and $I^{\mathrm{w}}_{\mathrm{meas}}$ is the measured ionization. A similar equation defines the pad estimator I_i^{p}.

A new energy loss estimator I is built from those two. This estimator is just the pad estimator for tracks that do not fulfil the requirement on the minimum number of isolated wire signals, otherwise it combines wire and pad information using the B.L.U.E. technique [12], taking into account the correlation of about 50% between the two measurements.

4.1 Electrons

For this analysis the momentum cut is lowered to $p > 2$ GeV/c with respect to the selection described in [10]. The requirement on the minimum number of isolated TPC wire signals is dropped, and a cut on the new energy loss estimator $I_e > -2$ is applied. This removes the dependence of the identification efficiency upon the track isolation, and hence the electron $p_\perp$. Compared to the previous selection, the new treatment of the energy loss information provides an increase in efficiency that goes from a few percent at high $p_\perp$ to about 30% at low $p_\perp$. The background increases marginally.

4.2 Muons

The momentum cut is lowered to $p > 2.5$ GeV/c. This still ensures that all muons reach the muon chambers but introduces a small dependence in the identification efficiency on the momentum. A dedicated study has been performed using $\gamma\gamma \to \mu^+\mu^-$ events (Sect. 6.4).

A cut on the polar angle $|\cos\theta| < 0.7$ is applied, which ensures that the muon is within the acceptance of both vertex detector layers. At least one VDET hit is required to be associated with the muon track, and the distance to the primary vertex in the plane orthogonal to the beam axis is required to satisfy $|d_0| < 2.5$ mm. This substantially reduces the contamination from muons coming from kaon and pion decays.

In addition a cut on the energy-loss estimator $I_\mu > -2$ is applied; this further reduces the background from misidentified kaons by more than a factor of two. The inefficiency for prompt muons introduced by these additional cuts is smaller than 1% in the angular region considered.

5 The analysis method

The lepton production rate in a sample of hemispheres with high b purity is dominated by the $b \to X\ell\nu$ and $b \to c \to X\ell\nu$ processes. In order to disentangle these two contributions, two different procedures are used, one based on the lepton kinematics, the other on the lepton charge. The two methods are described below.

5.1 Transverse momentum analysis

Sample $\mathcal{B}$, described in Sect. 3, contains a large number of nearly unbiased b decays. The lepton rate in such a sample can be directly interpreted in terms of the sum of the direct and cascade inclusive semileptonic b decays, weighted by their selection efficiencies, once contributions from other physics sources and misidentified leptons have been corrected for.

The study of the lepton rate as a function of the transverse momentum which discriminates the two components, allows the two branching ratios to be fitted simultaneously.

Therefore a measurement of $\mathrm{BR}(b \to X\ell\nu)$ and $\mathrm{BR}(b \to c \to X\ell\nu)$ can be obtained from a maximum likelihood fit to the number of leptons in each transverse momentum bin, as follows:

$$\mathcal{L} = \prod_i \frac{e^{-\mu_i}\,\mu_i^{n_i}}{n_i!}\ , \tag{1}$$

where the product runs over the transverse momentum bins, n_i is the number of leptons found in the data in each bin, μ_i is the expected number of leptons, which depends on the two branching ratios and contains the contributions from all the other sources of lepton candidates.

Equation (1) can be rewritten as

$$\mathcal{L} = \underbrace{\frac{e^{-\mu}\,\mu^N}{N!}}_{\text{counting}} \times \underbrace{\prod_{j=1}^{N} \mathcal{F}(p_\perp^j)}_{p_\perp \text{ spectrum}}\ , \tag{2}$$

where N is the total number of candidates observed in the data ($N = \sum_i n_i$), μ is the expected number ($\mu = \sum_i \mu_i$), and $\mathcal{F}(p_\perp)$ is the binned probability density function that gives the expected shape of the distribution of the candidates as a function of $p_\perp$ ($\mathcal{F}_i = \mu_i/\mu$). The product runs over the lepton candidates.

The expected number of candidates (μ) in the selected hemispheres (N_{hemi}) depends on the signal branching ratios multiplied by the average selection efficiencies $\epsilon_{b\to x}$, and on the rates of the other sources of lepton candidates:

$$\mu = N_{\mathrm{hemi}} \times \Big[\mathrm{BR}(b \to X\ell\nu)\epsilon_{b\to X\ell\nu} + \mathrm{BR}(b \to c \to X\ell\nu)\epsilon_{b\to c\to X\ell\nu} + \text{other sources}\Big]\ .$$

The expected $p_\perp$ shape depends on the shapes of the different components and their relative abundances:

$$\mathcal{F}(p_\perp) = f_{b\to X\ell\nu}\mathcal{F}^{b\to X\ell\nu}(p_\perp) + f_{b\to c\to X\ell\nu}\mathcal{F}^{b\to c\to X\ell\nu}(p_\perp) + \cdots$$

where the shapes $\mathcal{F}^i(p_\perp)$ are normalized to unity, the $b \to X\ell\nu$ fraction is written as

$$f_{b\to X\ell\nu} = \Big\{\Big(\mathrm{BR}(b \to X\ell\nu)\epsilon_{b\to X\ell\nu}\Big)\Big/ \Big(\mathrm{BR}(b \to X\ell\nu)\epsilon_{b\to X\ell\nu} + \mathrm{BR}(b \to c \to X\ell\nu) \times \epsilon_{b\to c\to X\ell\nu} + \text{other sources}\Big)\Big\}\ ,$$

and similar equations hold for all the components.

The part of the likelihood labelled as "counting" contains the information on the total rate, and is therefore sensitive to the (weighted) sum of the two branching ratios. It is affected by uncertainties on the lepton identification efficiency and background, as well as on the rates of other processes yielding leptons. It has little dependence on the modelling of the $p_\perp$ spectrum.

The part labelled as "$p_\perp$ spectrum" is sensitive to the relative contribution of the two signal sources, but almost insensitive to their overall normalization. It is heavily affected by uncertainties in the b decay modelling.

5.2 Charge correlation analysis

Another way of discriminating the $b \to X\ell\nu$ and $b \to c \to X\ell\nu$ components is to exploit the different correlation of the lepton and the parent quark charges. The second part of the likelihood in (2) can be replaced with a term containing the fraction of leptons that have the same or the opposite charge relative to a charge estimator built using tracks in the opposite hemisphere (*e.g.*jet charge).

However, such a method would have poor statistical power if applied to sample $\mathcal{B}$. The charge tag samples $\mathcal{P}$ and $\mathcal{J}$ are selected for this reason, somewhat relaxing the requirement on the b purity in favour of higher statistics and better charge tagging.

A likelihood function is constructed based on the counting part from sample $\mathcal{B}$ and the charge spectra of samples $\mathcal{P}$ and $\mathcal{J}$ as follows:

$$\mathcal{L} = \underbrace{\frac{e^{-\mu}\,\mu^N}{N!}}_{\text{counting }(\mathcal{B})} \times \underbrace{\mathcal{F}_{\mathcal{P}}^{N_{O_{\mathcal{P}}}}\,(1-\mathcal{F}_{\mathcal{P}})^{N_{S_{\mathcal{P}}}}}_{\text{charge }(\mathcal{P})} \times \underbrace{\mathcal{F}_{\mathcal{J}}^{N_{O_{\mathcal{J}}}}\,(1-\mathcal{F}_{\mathcal{J}})^{N_{S_{\mathcal{J}}}}}_{\text{charge }(\mathcal{J})}\,, \quad (3)$$

where $\mathcal{F}_{\mathcal{P}}$ is the expected fraction of lepton candidates with charge opposite to the charge tag of the other hemisphere in sample $\mathcal{P}$, $N_{O_{\mathcal{P}}}$ and $N_{S_{\mathcal{P}}}$ are the numbers of candidates with opposite and same charge found in the data. The same holds for sample $\mathcal{J}$.

The expected fractions $\mathcal{F}_{\mathcal{P}}$ and $\mathcal{F}_{\mathcal{J}}$ are sensitive to the relative contributions of the $b \to X\ell\nu$ and $b \to c \to X\ell\nu$ components and depend on the rate of correct tagging for the opposite hemisphere charge estimator, as well as on the background components.

5.3 Flavour composition of the selected samples

The flavour composition for each of the three samples is estimated as follows. The fraction $F_{\rm hemi}$ of single b-tagged hemispheres is measured from the data. The efficiency $\epsilon_{\rm c}$ for tagging charm events and the average efficiency $\epsilon_{\rm uds}$ for tagging light quark events are determined using simulated events, and the sample composition is calculated as

$$f^{\rm b}_{\rm hemi} = 1 - \frac{R_{\rm c}\epsilon_{\rm c} + (1 - R_{\rm b} - R_{\rm c})\epsilon_{\rm uds}}{F_{\rm hemi}}\,,$$
$$f^{\rm c}_{\rm hemi} = \frac{R_{\rm c}\epsilon_{\rm c}}{F_{\rm hemi}}\,,$$
$$f^{\rm uds}_{\rm hemi} = \frac{(1 - R_{\rm b} - R_{\rm c})\,\epsilon_{\rm uds}}{F_{\rm hemi}}\,,$$

where $R_{\rm b}$ and $R_{\rm c}$ [13] are the ratios of the $b\bar{b}$ and $c\bar{c}$ partial widths of the Z to the total hadronic width, taken from experimental measurements.

5.4 Charge tagging in samples $\mathcal{P}$ and $\mathcal{J}$

The terms $\mathcal{F}_{\mathcal{P}}$ and $\mathcal{F}_{\mathcal{J}}$ in (3) are written in terms of the probabilities that the charge of the parent quark in the hemisphere opposite to the lepton candidate is correctly tagged. These probabilities for b or $\bar{\rm b}$ quarks $P_{\rm b\bar{b}}$, discussed in Sect. 3, are measured from the data by means of a double-tag method. The description below applies to both samples $\mathcal{P}$ and $\mathcal{J}$.

The charge-tagging selection cut is applied to both hemispheres, and the events selected are split into three classes: those in which the two hemispheres have opposite charge, and those in which have the same charge, positive or negative. The three fractions $F^{\rm oc}$, F^{++} and F^{--} can be written as

$$F^{\rm oc} = f^{\rm b}_{\rm evt}F^{\rm oc}_{\rm b} + f^{\rm c}_{\rm evt}F^{\rm oc}_{\rm c} + f^{\rm uds}_{\rm evt}F^{\rm oc}_{\rm uds}\,, \quad (4)$$

where $f^{\rm b}_{\rm evt}$, $f^{\rm c}_{\rm evt}$ and $f^{\rm uds}_{\rm evt}$ are the contributions of b, c and light flavour events to this sample, with similar equations for F^{++} and F^{--}. The different flavour contributions are measured with the same procedure used to estimate the hemisphere sample composition (Sect. 5.3):

$$f^{\rm b}_{\rm evt} = 1 - \frac{R_{\rm c}\zeta_{\rm c} + (1 - R_{\rm b} - R_{\rm c})\zeta_{\rm uds}}{F_{\rm evt}}\,,$$
$$f^{\rm c}_{\rm evt} = \frac{R_{\rm c}\zeta_{\rm c}}{F_{\rm evt}}\,,$$
$$f^{\rm uds}_{\rm evt} = \frac{(1 - R_{\rm b} - R_{\rm c})\,\zeta_{\rm uds}}{F_{\rm evt}}\,, \quad (5)$$

where $F_{\rm evt}$ is the fraction of events with both hemispheres tagged in the data, and $\zeta_{\rm c}$ and $\zeta_{\rm uds}$ are the charm and light quark event efficiencies determined from the simulation.

The fractions $F^{\rm oc}_{\rm c}$ ($F^{++}_{\rm c}$, $F^{--}_{\rm c}$) and $F^{\rm oc}_{\rm uds}$ ($F^{++}_{\rm uds}$, $F^{--}_{\rm uds}$) of events with opposite (same) hemisphere charges in charm and light quark events are taken from the simulation, and (4) is solved for $F^{\rm oc}_{\rm b}$ ($F^{++}_{\rm b}$, $F^{--}_{\rm b}$).

In order to extract $P_{\rm b\bar{b}}$ from $F^{\rm oc}_{\rm b}$, several effects must be considered.

- Because of the interaction of particles with the detector material, the probability for correct charge tagging is different for b and $\bar{\rm b}$ quarks. The difference can be defined as $P^{\rm DT}_{\rm b} = P^{\rm DT}_{\rm b\bar{b}}(1-\epsilon)$, $P^{\rm DT}_{\bar{\rm b}} = P^{\rm DT}_{\rm b\bar{b}}(1+\epsilon)$, where $P^{\rm DT}_{\rm b\bar{b}}$ is the average probability of correct charge tagging in the double-tagged sample selected.
- The probabilities of correct charge tagging in the two hemispheres are not independent. The correlation ρ is defined so that a hemisphere opposite to one in which the charge was correctly tagged has the probability of correct charge tagging enhanced by a factor $(1+\rho)$.
- The sample used for the branching ratio measurement includes hemispheres for which the opposite one did not fulfil the selection cuts. The selection in the opposite hemisphere has some correlation with the charge tagging probability of the hemisphere considered, therefore the parameter which is measured with the double tag method requires a further correction, α, as explained below.

With all these effects taken into account, $P^{\rm DT}_{\rm b\bar{b}}$ is related to $F^{\rm oc}_{\rm b}$ via

$$F^{\rm oc}_{\rm b} = \left(P^{\rm DT}_{\rm b\bar{b}}\right)^2 + \left(1 - P^{\rm DT}_{\rm b\bar{b}}\right)^2 + 2\left(P^{\rm DT}_{\rm b\bar{b}}\right)^2\left(\rho - \epsilon^2 - \epsilon^2\rho\right), \quad (6)$$

Table 1. Estimated contributions to the systematic uncertainties on BR(b → Xℓν) and BR(b → c → Xℓν)). Results for both transverse momentum and charge correlation analyses are given. Uncertainties related to the modelling of semileptonic decays are shown separately in Table 2. All values are given in units of 10^{-2}

	Δ[BR(b → Xℓν)]		Δ[BR(b → c → Xℓν)]	
Source	$p_\perp$	Charge	$p_\perp$	Charge
R_b	negl.	negl.	negl.	negl.
R_c	± 0.005	∓ 0.007	∓ 0.002	± 0.017
$N(g \to b\bar{b})$	∓ 0.002	∓ 0.002	∓ 0.002	∓ 0.001
$N(g \to c\bar{c})$	∓ 0.001	∓ 0.006	∓ 0.014	∓ 0.006
electron ID efficiency	∓ 0.063	∓ 0.081	∓ 0.087	∓ 0.056
γ conversions	± 0.003	∓ 0.006	∓ 0.022	∓ 0.008
electron bkg	± 0.004	∓ 0.007	∓ 0.026	∓ 0.009
muon ID efficiency	± 0.065	± 0.063	± 0.039	± 0.039
muon bkg	± 0.002	∓ 0.013	∓ 0.037	∓ 0.015
$BR(b \to c \to X\ell\nu)|_\ell$	± 0.004	± 0.022	± 0.002	∓ 0.026
BR(b → J/ψ (ψ') → ℓℓ)	negl.	negl.	negl.	negl.
BR(b → τ → ℓ)	∓ 0.017	∓ 0.043	∓ 0.053	∓ 0.011
BR(b → W → $\bar{c}$ → ℓ)	± 0.010	∓ 0.223	∓ 0.407	∓ 0.039
BR(c → Xℓν)	negl.	∓ 0.016	∓ 0.009	± 0.016
BR(b → X_uℓ)	∓ 0.032	∓ 0.022	± 0.013	∓ 0.004
b fragmentation	∓ 0.074	∓ 0.089	∓ 0.120	∓ 0.101
c fragmentation	± 0.001	± 0.005	negl.	∓ 0.005
ϵ_c sample $\mathcal{B}$	± 0.027	± 0.015	∓ 0.009	∓ 0.010
ϵ_{uds} sample $\mathcal{B}$	± 0.015	± 0.016	± 0.012	± 0.011
ϵ_c sample $\mathcal{J}$	-	∓ 0.018	-	± 0.029
ϵ_{uds} sample $\mathcal{J}$	-	negl.	-	negl.
ϵ_c sample $\mathcal{P}$	-	∓ 0.012	-	± 0.019
ϵ_{uds} sample $\mathcal{P}$	-	negl.	-	negl.
c charge tag rate	-	± 0.036	-	∓ 0.057
b charge tag rate	-	± 0.069	-	∓ 0.109
Mixing in b → Xℓν	-	± 0.035	-	∓ 0.055
Mixing in b → c → Xℓν	-	∓ 0.055	-	± 0.087
bkg charge correlation	-	± 0.027	-	∓ 0.043
b tag - lept correlation	± 0.006	∓ 0.007	∓ 0.025	∓ 0.005
Total	± 0.128	± 0.290	± 0.443	± 0.212

where ϵ can be written as

$$\epsilon = \frac{F_b^{++} - F_b^{--}}{2P_{b\bar{b}}^{DT}}. \quad (7)$$

Equation (6) and (7) can be solved for $P_{b\bar{b}}^{DT}$ and ϵ taking for ρ the estimate provided by the simulation. Then $P_{b\bar{b}}$ is calculated as

$$P_{b\bar{b}} = (1-\alpha)P_{b\bar{b}}^{DT}\ , \quad (8)$$

in terms of a bias correction α also taken from simulated events. Both α and ρ are found to be smaller than 1%.

6 Sources of systematic errors

In this section the sources of possible systematic effects are discussed. The estimated uncertainties are summarized in Tables 1 and 2.

Table 2. Estimated contributions to the systematic uncertainties on BR(b → Xℓν) and BR(b → c → Xℓν)) related to the modelling of semileptonic decays. The uncertainty in the modelling of direct b → Xℓν decays is estimated by adding in quadrature the uncertainties from the rate of the different charmed mesons, inflated by 25%, and the uncertainties from the production rates of B_s^0 mesons and b baryons, as discussed in Sect. 6.15. Results for both transverse momentum and charge correlation analyses are shown. All values are given in units of 10^{-2}

	Δ[BR(b → Xℓν)]		Δ[BR(b → c → Xℓν)]	
Source	$p_\perp$	Charge	$p_\perp$	Charge
Dℓν	± 0.012	± 0.022	± 0.029	± 0.013
D⋆ℓν	∓ 0.008	± 0.077	± 0.035	± 0.010
Inclusive $D^{(\star)}X\ell\nu$	± 0.254	± 0.086	∓ 0.265	∓ 0.004
$D_1\ell\nu$	∓ 0.068	∓ 0.028	± 0.056	∓ 0.007
$D_2^\star\ell\nu$	∓ 0.047	∓ 0.018	± 0.040	∓ 0.006
Broad states	± 0.327	± 0.169	∓ 0.191	± 0.052
B_s^0 fraction	± 0.049	± 0.060	± 0.063	± 0.048
Baryon fraction	∓ 0.025	∓ 0.012	± 0.059	± 0.044
b → Xℓν modelling	± 0.426	± 0.202	± 0.348	± 0.085
c → Xℓν modelling	$^{-0.087}_{+0.072}$	$^{-0.038}_{+0.021}$	$^{-0.037}_{+0.020}$	$^{-0.117}_{+0.063}$
b → D modelling	$^{-0.072}_{+0.060}$	$^{-0.002}_{+0.001}$	$^{-0.055}_{+0.049}$	$^{+0.058}_{-0.050}$
Total modelling	$^{+0.436}_{-0.441}$	$^{+0.204}_{-0.206}$	$^{+0.353}_{-0.355}$	$^{+0.117}_{-0.156}$

6.1 Z partial widths to $b\bar{b}$ and $c\bar{c}$

The values of R_b and R_c are used in the derivation of the sample compositions of the three hemisphere samples, and in the calculation of $P_{b\bar{b}}^{\mathcal{P}}$ and $P_{b\bar{b}}^{\mathcal{J}}$. The most recent averages are taken [13], $R_b = 0.21653 \pm 0.00069$ and $R_c = 0.1709 \pm 0.0034$, and the experimental errors are considered as sources of systematic uncertainty.

6.2 Heavy quarks from gluon splitting

Charm and bottom quark pairs may be produced from the splitting of hard gluons. The heavy flavour hadrons resulting from this process have a significantly softer energy spectrum and thus give rise to a source of prompt leptons with kinematic properties substantially different from those produced by heavy hadrons from direct Z decay. In addition, leptons originating from gluons splitting to heavy quarks have a random charge correlation with the charge estimators defined in the opposite hemisphere.

The latest world average values are used for the number of gluons splitting to heavy quarks per hadronic Z decay [14],

$$N(g \to b\bar{b}) = 0.00254 \pm 0.00051\ ,$$
$$N(g \to c\bar{c}) = 0.0296\ \ \pm 0.038\ ,$$

and the experimental errors are used to estimate the associated uncertainty.

6.3 Electron identification efficiency and background

The electron identification efficiency is measured from data using photon conversions in the detector material. Correction factors are derived, with respect to the Monte Carlo, for the dependence on momentum, transverse momentum and polar angle. These factors typically differ from unity by less than 1%. The associated systematic uncertainty is estimated by removing the corrections.

The background from hadron misidentification is estimated by removing the cut on the energy loss, and studying the shape of the I estimator. This study is performed on data and Monte Carlo and no significant deviation is observed. An uncertainty of 20% on the backgroud level is assigned from the statistical precision of the method.

The background from unidentified photon conversions is estimated by studying the shape of the variable

$$\rho_\gamma \ = q\, d_0\, p_{\mathrm{T}} \ ,$$

where q is the charge of the electron, d_0 is the distance of closest approach to the primary vertex in the xy plane signed according to the track angular momentum around the origin, and p_{T} is the component of the track momentum transverse to the beam axis. The variable ρ_γ is expected to be zero for prompt electrons and proportional to the square of the materialization radius for electrons coming from photon conversions. The study of the positive tail of the distribution yields a correction factor of 1.05 to be applied to the simulation, with a statistical error of 0.02. The correction factor is removed to estimate the systematic uncertainty.

6.4 Muon identification efficiency and background

The identification efficiency for high energy muons is measured from the data using Z decays to muon pairs, as a function of polar and azimuthal angle. Simulated events are reweighted to reproduce the measured efficiencies. Correction factors are typically a few per mil.

Simulated events show some dependence of the identification efficiency upon the muon momentum for momenta around 3 GeV/c. This effect is also checked on real data using $\gamma\gamma \to \mu^+\mu^-$ events. Additional correction factors, of order 1 to 2% are derived for muons with momenta between 2.5 GeV/c and 4 GeV/c. The shift observed when the corrections factors are removed is used as an estimate of the systematic uncertainty.

The main background for muon candidates is due to misidentified pions as well as pions decaying before entering the calorimeters. The corresponding contributions for kaons are substantially reduced by the cut on the measured energy loss, and are estimated to be a factor of four smaller.

In order to check the background rate from data, $\mathrm{K}^0_{\mathrm{S}} \to \pi^+\pi^-$ decays are selected in hadronic events to yield a 99% pure sample of pions. The muon identification procedure is applied to these tracks, and the selection efficiency is compared between data and Monte Carlo. Agreement is found within the statistical precision of the test, which is 5%. The test is repeated applying different $\mathcal{B}_{\mathrm{tag}}$ cuts in the hemisphere opposite to the $\mathrm{K}^0_{\mathrm{S}}$ candidate in order to check for a possible dependence on the flavour. No trend is observed.

The uncertainty of 5% estimated from the check with $\mathrm{K}^0_{\mathrm{S}} \to \pi^+\pi^-$ is enlarged to 10% for the assignment of a systematic error to the muon background. This allows for additional uncertainties from the smaller kaon component, as well as possible differences between data and simulation in the production rates and kinematic properties of pions and kaons in b events.

6.5 Specific $\mathrm{b} \to \mathrm{c} \to \mathrm{X}\ell\nu$ correction

The $\mathrm{b} \to \mathrm{c} \to \mathrm{X}\ell\nu$ rate is in principle different in transitions where the W from the b hadron decays leptonically, $\mathrm{BR}(\mathrm{b} \to \mathrm{c} \to \mathrm{X}\ell\nu)|_\ell$, or hadronically, $\mathrm{BR}(\mathrm{b} \to \mathrm{c} \to \mathrm{X}\ell\nu)|_{\mathrm{h}}$. The fit could yield a biased result for the average $\mathrm{BR}(\mathrm{b} \to \mathrm{c} \to \mathrm{X}\ell\nu)$ if the acceptance were different for the two cases. This effect is investigated by changing in the simulation the relative population of the two species and recalculating all efficiencies and spectra. The $\mathrm{BR}(\mathrm{b} \to \mathrm{c} \to \mathrm{X}\ell\nu)|_\ell$ is increased to a conservative 20% and the $\mathrm{BR}(\mathrm{b} \to \mathrm{c} \to \mathrm{X}\ell\nu)|_{\mathrm{h}}$ is decreased accordingly. The shift observed in the fitted values is taken as an estimate of the associated systematic error.

6.6 Other sources of prompt leptons

The rates of leptons coming from J/ψ and from intermediate τ decays used for this analysis are [14]

$$\mathrm{BR}(\mathrm{b} \to \mathrm{J}/\psi\ (\psi') \to \ell\ell) = 0.00072 \ \pm 0.00006 \ ,$$
$$\mathrm{BR}(\mathrm{b} \to \tau \to \ell) = 0.00419 \pm 0.00055 \ .$$

Leptons produced from cascade b decays where the intermediate charm is produced from a $\mathrm{W} \to \bar{\mathrm{c}}\mathrm{s}$ transition, denoted $\mathrm{b} \to \mathrm{W} \to \bar{\mathrm{c}} \to \ell$, are also a background to the analysis. They affect most directly the result for $\mathrm{BR}(\mathrm{b} \to \mathrm{c} \to \mathrm{X}\ell\nu)$ in the transverse momentum analysis, as they have kinematic properties similar to $\mathrm{b} \to \mathrm{c} \to \mathrm{X}\ell\nu$ decays. On the other hand in the charge correlation analysis only the value of $\mathrm{BR}(\mathrm{b} \to \mathrm{X}\ell\nu)$ depends on the rate of these transitions since the correlation between the charge of the lepton and the charge of the parent quark is the same as in $\mathrm{b} \to \mathrm{X}\ell\nu$ direct decays. The value used is [14]

$$\mathrm{BR}(\mathrm{b} \to \mathrm{W} \to \bar{\mathrm{c}} \to \ell) \ = \ 0.0162 \pm 0.0044 \ .$$

The semileptonic decays of charmed hadrons in the residual background of $\mathrm{c\bar{c}}$ events contribute to the total observed lepton yield. The LEP average value [13] is taken:

$$\mathrm{BR}(\mathrm{c} \to \ell) \ = \ 0.0984 \pm 0.0032 \ .$$

All the above sources of leptons are subtracted from the total lepton yield.

The rate of lepton production in charmless semileptonic b decays, $b \to X_u \ell$, mainly affects the high end of the $p_\perp$ spectrum. A variation of this contribution relative to the total $BR(b \to X \ell \nu)$ is included in the systematic error calculation. The value used in this analysis is [15]

$$BR(b \to X_u \ell) \;=\; 0.00167 \pm 0.00055 \; .$$

6.7 Fragmentation of b quarks

The scaled energy spectrum of b hadrons in the simulation is modified in order to reproduce the spectrum reconstructed in the model-independent analysis of [6].

The statistical and systematic uncertainties on the population of each energy bin are propagated to the measured branching ratios, taking into account bin-to-bin correlations. The systematic errors on the energy spectrum due to the uncertainty on the charmed meson species produced in B meson decays are not considered here, as they are correlated with the uncertainty on the modelling of semileptonic decays (Sect. 6.15).

The correction factors derived from the comparison of the measured and simulated energy spectra of B mesons are also applied to B_s^0 mesons and b baryons.

6.8 Fragmentation of c quarks

Charm fragmentation is simulated using the Peterson et al. model [16]. The parameter ε_c, which controls the shape of the function, is adjusted to reproduce the measured value of the mean scaled energy of weakly-decaying charmed hadrons, $\langle x_c \rangle = 0.484 \pm 0.008$ [14], and then varied by its uncertainty.

6.9 Charm and light quark background

The calculation of the sample compositions described in Sect. 5.3 relies on the simulation for estimates of the charm and light quark hemisphere selection efficiencies. For samples $\mathcal{B}$ and $\mathcal{J}$ the estimate of the uncertainty on the background efficiencies follows the lines of [9], where all the relevant physics parameters in the Monte Carlo have been reweighted. The values used for this analysis are

$$\begin{aligned} \epsilon_c^{\mathcal{B}} &= 0.00939 \pm 0.00094 \qquad \epsilon_{uds}^{\mathcal{B}} &= 0.00060 \pm 0.00015 \; , \\ \epsilon_c^{\mathcal{J}} &= 0.0439 \;\pm 0.0022 \qquad \epsilon_{uds}^{\mathcal{J}} &= 0.0054 \;\pm 0.0008 \; . \end{aligned}$$

For sample $\mathcal{P}$ the dominant sources of uncertainty are the charm semileptonic branching fraction and decay modelling, for charm hemispheres, and lepton background for light quark hemispheres. The corresponding values and errors are

$$\epsilon_c^{\mathcal{P}} \;=\; 0.0108 \;\pm 0.0011 \qquad \epsilon_{uds}^{\mathcal{P}} \;=\; 0.0016 \;\pm 0.0003 \; .$$

6.10 Charge tagging in charm and light quark hemispheres

The fractions of opposite charge charm and light quark hemispheres entering (4) are taken from the simulation. The difference between F^{++} and F^{--} for these flavours is neglected in the analysis, therefore they are determined once F^{oc} is obtained.

In sample $\mathcal{P}$, F_c^{oc} is determined by the relative amounts of true and fake leptons selected, and by the degree of correlation between the charge of fake leptons and the charge of the c quark. The rates of lepton production from c hadron semileptonic decays and from hadron misidentification are varied within their estimated uncertainties (Sects. 6.3, 6.4 and 6.6). The charge correlation for fake leptons is set to zero and half of the difference in F_c^{oc} is taken as an estimate of the related uncertainties. Adding the uncertainties from the three sources in quadrature yields $F_c^{oc} = 0.87 \pm 0.04$ in sample $\mathcal{P}$, corresponding to $P_{c\bar{c}}^{\mathcal{P}} = 0.93 \pm 0.02$.

For sample $\mathcal{J}$ an estimate of the uncertainty on F_c^{oc} is obtained by comparing the value with F_b^{oc}. For charm hemispheres, the correlation between the charge of the quark and the sign of the estimator is stronger than in the case of b hemispheres. This is valid separately for the two estimators Q_p and Q_s. For the first, the reason is the higher charm quark charge. In the case of Q_s, the effect is due to the b-tagging cut which selects charm hemispheres with particularly long lifetime, and to the smaller charged particle multiplicity of c hadron decays compared to b hadron decays. The systematic uncertainty is evaluated by setting the charge correlation for charm hemispheres equal to that for b hemispheres and taking half of the difference as the systematic uncertainty; this procedure yields $F_c^{oc} = 0.64 \pm 0.02$ in sample $\mathcal{J}$, corresponding to $P_{c\bar{c}}^{\mathcal{J}} = 0.77 \pm 0.02$.

In light quark events, F_{uds}^{oc} is still somewhat larger than 0.5 due to the correlation of the estimator with the parent quark charge, for both samples. However the systematic uncertainty obtained by setting it equal to 0.5 is negligible.

6.11 Charge tagging in b hemispheres

Besides the sources already considered, the uncertainty on $P_{b\bar{b}}$ also depends on the uncertainties on F^{oc}, F^{++}, F^{--}, F_{evt}, ζ_c, ζ_{uds}, ρ and α appearing in (4)–(8).

The statistical errors on F^{oc}, F^{++}, F^{--} and F_{evt}, which are measured from the data, are propagated to the results of the fit and included in the statistical errors on the branching ratios.

For sample $\mathcal{J}$ the values of ρ and α measured in the simulated events are 0.0096 and 0.0063, respectively. For sample $\mathcal{P}$, α is found to be 0.0062, while there is no significant correlation between the two hemispheres. The associated systematic uncertainty is estimated by setting ρ and α to zero and taking half of the observed shift.

The uncertainties from ζ_c and ζ_{uds} are negligible.

6.12 Neutral B meson mixing

The mixing of neutral B mesons contributes to the degradation of the correlation between the charge of the lepton and the charge of the parent b quark produced in the Z decay. The LEP average $\bar{\chi} = 0.1194 \pm 0.0043$ [13] is used as input in the likelihood. This value is interpreted as the average mixing rate for the b hadron mixture from $b \to X\ell\nu$ decays.

The relative population of B_d^0 and B^+ mesons is not equal in $b \to c \to X\ell\nu$ decays, due to the different semileptonic branching ratios of D^+ and D^0 mesons, leading to an effectively higher value of the average mixing parameter $\bar{\chi}' = \bar{\chi}\,(1+\delta)$. The value $\delta = 0.13$ is estimated from the simulation and is varied by 50% to estimate the systematic uncertainty.

As a consequence the expected fraction of events with hemispheres of opposite sign for the $b \to X\ell\nu$ and $b \to c \to X\ell\nu$ components is

$$\begin{aligned} b \to X\ell\nu\colon\ \mathcal{F} &= P_{b\bar{b}}\,(1-\bar{\chi}) + (1-P_{b\bar{b}})\,\bar{\chi}\ , \\ b \to c \to X\ell\nu\colon\ \mathcal{F} &= P_{b\bar{b}}\,\bar{\chi}' + (1-P_{b\bar{b}})\,(1-\bar{\chi}')\ . \end{aligned}$$

6.13 Charge correlation for lepton background

Leptons coming from kaon and pion decays in flight as well as misidentified kaons and pions retain some information about the charge of the primary quark, both in charm and in b events. This effect must be taken into account when evaluating the opposite-charge and same-charge fractions in the charge correlation analysis. The rate at which the information about the quark charge is retained is measured in the Monte Carlo. The systematic uncertainty is evaluated by taking half of the difference between the Monte Carlo value and no charge correlation.

6.14 Hemisphere-hemisphere correlation

The b-tagging efficiency is affected by the presence of a lepton in the hemisphere opposite to that used for the flavour tagging, in a way that depends on both the momentum and the transverse momentum of the lepton. In particular, hemispheres opposite to a high momentum lepton are more likely to satisfy the b-tagging cut since such leptons are likely to be produced in events with little gluon emission, where both b hadrons have high momentum. The b-tagging efficiency for those hemispheres is then higher than expected in an unbiased sample of hemispheres.

The ratio $R = \epsilon_b^l/(\epsilon_b \times \epsilon_l)$ is determined from simulated events, where ϵ_b and ϵ_l are respectively the b-tagging efficiency and the probability of finding a lepton in a b hemisphere while ϵ_b^l is the probability that in the same event one hemisphere is b-tagged and in the opposite hemisphere one lepton is selected. The dependence of R upon the lepton momentum is irrelevant for the analysis, while the overall value affects the part of the likelihood labelled as "counting" in (2) and (3), and the dependence on the lepton transverse momentum affects the part labelled as "$p_\perp$ spectrum" in (2). The quantity R is therefore determined as a function of the lepton $p_\perp$, for the different sources of lepton candidates, and the corresponding correction factors are applied in the analysis. Deviations from unity are typically smaller than 1%. The corresponding systematic uncertainty is estimated by removing the corrections.

Table 3. Branching ratios for semileptonic decays of B mesons with different charmed mesons in the final state

Process	BR (%)
$B \to D\ell\nu$	1.95 ± 0.27
$B \to D^\star\ell\nu$	5.05 ± 0.25
$B \to D^{(\star)}X\ell\nu$	2.7 ± 0.7
with $B \to D_1\ell\nu$	0.63 ± 0.11
with $B \to D_2^\star\ell\nu$	0.23 ± 0.09

6.15 Modelling of direct semileptonic b decays

In the past, in all measurements of the inclusive $b \to X\ell\nu$ rate the decay kinematics were modelled using the ACCMM spectrum, and the associated systematic uncertainty was estimated from the shift observed using the ISGW and ISGW** spectra, as proposed in [17].

In this work a different approach is used, based on the available measurements of the B meson decay rates into the different charm hadron final states. B^0 and B^+ mesons decay semileptonically into D, $D^\star$ and $D^{\star\star}$ mesons, as well as non-resonant $D^{(\star)}\pi$ final states. Leptons coming from each of these components have a different energy spectrum so that the shape of the inclusive $B \to X\ell\nu$ spectrum depends on the branching fractions of B^0 and B^+ into the various charmed species. In the simulation, $B \to D\ell\nu$ and $B \to D^\star\ell\nu$ decays are modelled according to [18]. All $B \to D^{\star\star}\ell\nu$ decays follow the free-quark matrix element, and for non-resonant decays a simple phase-space model is used. As the lepton spectra from the various decay channels are substantially different (particularly large is the difference between 3-body and 4-body decays), the overall uncertainty in the spectrum is dominated by the proportions of the final states, rather than the detailed modelling of each individual channel. Thus the latter is neglected.

The fractions of D, $D^\star$, D_1, and $D_2^\star$ in the simulation are reweighted using the latest measured values [15,19] reported in Table 3. The broad $D^{\star\star}$ states are assumed to be equal to the sum of the narrow D_1 and $D_2^\star$ states, and the non-resonant $D^{(\star)}\pi$ decays account for the rate needed in order to add up to the measured inclusive $D^{(\star)}X$ branching ratio.

The systematic uncertainty is evaluated by varying the measured branching fractions within their estimated errors. Additionally the rate of the broad states is set to zero and compensated entirely with the non-resonant $D^{(\star)}\pi$ states. In each case, the B meson energy spectrum measured in [6] is used, thus taking into account the correla-

tion with the present analysis. This approach renders the analysis presented independent of the modelling of the b fragmentation in the simulation.

The energy spectra obtained with this procedure for the mixture of electrons and muons used in the analysis are compared in Fig. 4 with the inclusive spectra given in [17]. In Fig. 5 the effect of the corrections applied to estimate the systematic uncertainty is shown. The spectra resulting from this semi-exclusive treatment always lie between the softest (ISGW**) and hardest (ISGW) spectra.

The procedure described applies to B^0 and B^+ decays, which represent about 80% of the sample. Uncertainties in the production rates of B_s^0 mesons and b baryons can affect the analysis to the extent that their decay kinematics differ from those of B^0 and B^+ mesons. The B_s^0 and b baryon production rates are reweighted to the latest experimental results, $f_{B_s^0} = 0.094 \pm 0.022$ and $f_{b-baryon} = 0.101 \pm 0.018$ [15]. Uncertainties in the modelling of B_s^0 and b baryon decays are accounted for by enlarging the uncertainties from the branching ratios of Table 3 by 25%. Finally, the observed shifts on BR($b \to X\ell\nu$) and BR($b \to c \to X\ell\nu$) are symmetrized and added in quadrature.

6.16 Modelling of $c \to X\ell\nu$ and $b \to c \to X\ell\nu$ decays

The $c \to X\ell\nu$ decay spectrum is obtained by means of a combined fit to DELCO [20] and MARK III [21] data, performed using the ACCMM model and varied as described in [17].

In order to describe $b \to c \to X\ell\nu$ decays, the model proposed for $c \to X\ell\nu$ is combined with the measured $b \to D$ spectrum from CLEO [22] following the procedure of [17].

7 Results

The results obtained with the transverse momentum analysis are

$$\begin{aligned} \mathrm{BR}(b \to X\ell\nu) &= 0.1107 \pm 0.0007_{\,\mathrm{stat}} \pm 0.0013_{\,\mathrm{syst}} \\ &\quad \pm 0.0044_{\,\mathrm{model}} , \\ \mathrm{BR}(b \to c \to X\ell\nu) &= 0.0752 \pm 0.0010_{\,\mathrm{stat}} \pm 0.0044_{\,\mathrm{syst}} \\ &\quad \pm 0.0035_{\,\mathrm{model}} , \end{aligned}$$

with a statistical correlation of -0.45. The fitted spectrum is compared to the $p_\perp$ distribution observed in the data in Fig. 6, where the contributions of the two signal processes are also shown.

The charge correlation analysis gives

$$\begin{aligned} \mathrm{BR}(b \to X\ell\nu) &= 0.1057 \pm 0.0011_{\,\mathrm{stat}} \pm 0.0029_{\,\mathrm{syst}} \\ &\quad \pm 0.0020_{\,\mathrm{model}} , \\ \mathrm{BR}(b \to c \to X\ell\nu) &= 0.0830 \pm 0.0016_{\,\mathrm{stat}} \\ &\quad \pm 0.0021_{\,\mathrm{syst}}\, {}^{+0.0012}_{-0.0016\,\mathrm{model}} , \end{aligned}$$

with a statistical correlation of -0.76. Since this method does not use the information from the lepton $p_\perp$, the $p_\perp$ spectrum can be extracted from the data by repeating the charge correlation analysis in each $p_\perp$ bin. The values of BR($b \to X\ell\nu$) and BR($b \to c \to X\ell\nu$) measured in each $p_\perp$ bin are then used to reweight the Monte Carlo spectrum previously corrected as described in Sect. 6.15. In Fig. 7 the $b \to X\ell\nu$ and $b \to c \to X\ell\nu$ spectra shapes from the data are compared with the Monte Carlo. The

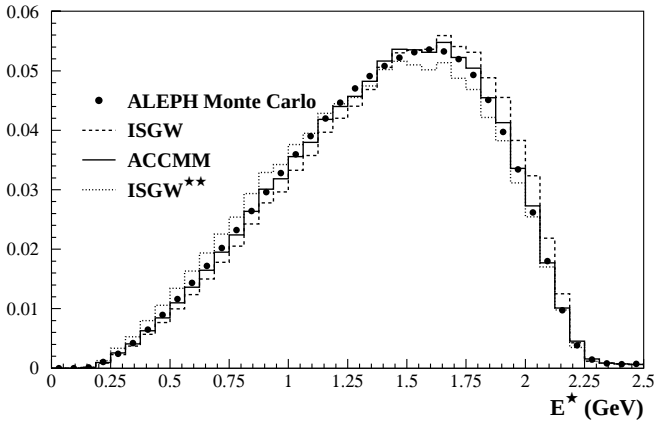

Fig. 4. Lepton energy spectrum in the b hadron rest frame. The histograms show the distributions obtained after reweighting with the ACCMM, ISGW and ISGW** models. The dots show the spectrum after correcting the Monte Carlo by following the procedure described in Sect. 6.15 using the central value of the branching ratios listed in Table 3

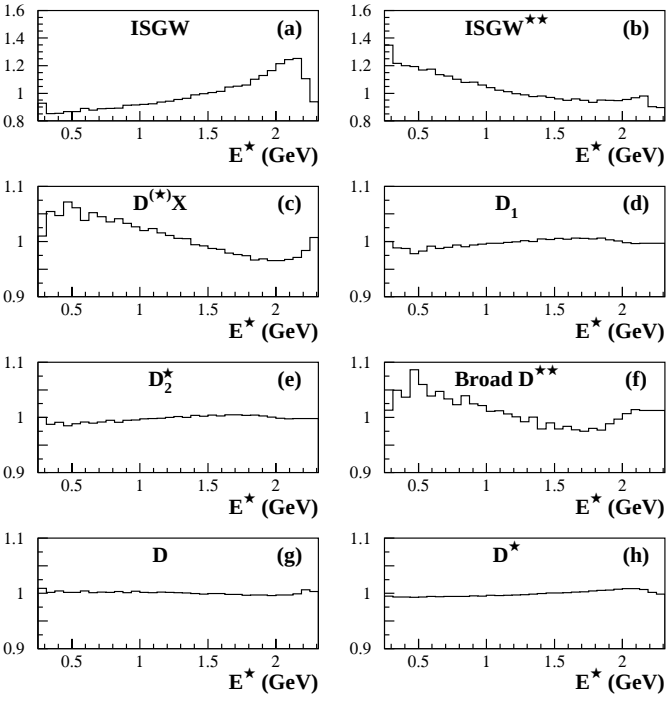

Fig. 5a–h. The plots **a** and **b** show the ratio between the lepton spectra given by the ISGW and ISGW** models and the spectrum obtained by correcting the Monte Carlo using the central value of the branching ratios listed in Table 3. Histograms **c**–**h** show the effect on the spectrum due to the variation by one standard deviation of each component with respect to the central value

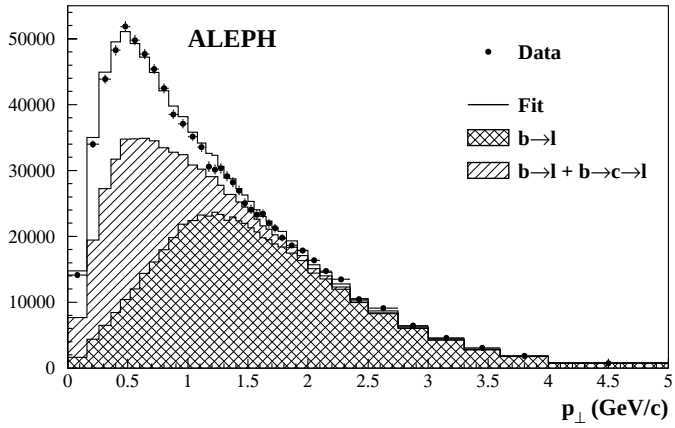

Fig. 6. Comparison between the lepton $p_\perp$ spectrum measured in the data and the result of the fit. The contribution from $b \to X\ell\nu$ as well as the sum of $b \to X\ell\nu$ and $b \to c \to X\ell\nu$ are shown. The error bars show statistical errors on the data

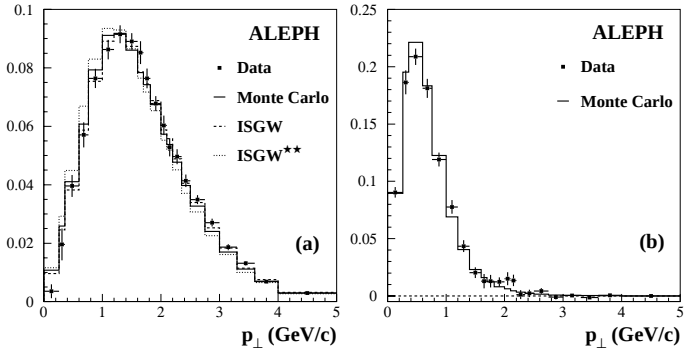

Fig. 7. Comparison between the lepton $p_\perp$ spectra measured in the data with the charge correlation analysis and that expected from simulation. **a** $b \to X\ell\nu$; data are compared with the simulation corrected as described in Sect. 6.15, ISGW and ISGW** models. **b** $b \to c \to X\ell\nu$. All the spectra are normalized to unit area

discrepancy observed reflects the difference between the results obtained with the two methods.

The differences can be quantified taking into account the correlation between systematic errors, as $\Delta_{b\to X\ell\nu} = 0.0049 \pm 0.0036$ (total error, of which 0.0025 is due to modelling) and $\Delta_{b\to c\to X\ell\nu} = 0.0077 \pm 0.0056$ (total error, of which 0.0039 is due to modelling). The two results are therefore consistent within 1.4 times the total uncorrelated error.

The statistical errors are correlated and smaller than the systematic errors. In the calculation of the average, maximal statistical correlation is assumed between the two measurements, i.e. 81% for $BR(b \to X\ell\nu)$ and 85% for $BR(b \to c \to X\ell\nu)$, which leads to a slight overestimate of the statistical errors. The weights used to calculate the average are $W_{b\to X\ell\nu}(p_\perp) = 0.25$, $W_{b\to X\ell\nu}(\text{charge}) = 0.75$, $W_{b\to c\to X\ell\nu}(p_\perp) = 0.15$, $W_{b\to c\to X\ell\nu}(\text{charge}) = 0.85$. They are determined by minimizing the total error (B.L.U.E. technique [12]). The resulting average values are

$$\begin{aligned} BR(b \to X\ell\nu) = 0.1070 &\pm 0.0010_{\,\text{stat}} \pm 0.0023_{\,\text{syst}} \\ &\pm 0.0026_{\,\text{model}} , \\ BR(b \to c \to X\ell\nu) = 0.0818 &\pm 0.0015_{\,\text{stat}} \\ &\pm 0.0022_{\,\text{syst}}\ ^{+0.0010}_{-0.0014\,\text{model}} . \end{aligned}$$

7.1 Consistency checks

The analysis was performed seperately for each year of data taking, to check for possible detector-related effects. The results are consistent throughout the whole LEP I period. The analysis was also performed using electron and muon candidates separately. The two species of leptons have different uncertainties in the selection efficiency and in the rate of background. The tighter selection cut applied on the muon momentum is reflected in a different dependence on modelling. The results are consistent within errors as shown by their differences quoted below.

Transverse momentum analysis:

$$\begin{aligned} \Delta^{e-\mu}_{b\to X\ell\nu} = -0.0029 &\pm 0.0013_{\,\text{stat}} \pm 0.0018_{\,\text{syst}} \\ &\pm 0.0002_{\,\text{model}} , \\ \Delta^{e-\mu}_{b\to c\to X\ell\nu} = \ \ 0.0017 &\pm 0.0020_{\,\text{stat}} \pm 0.0021_{\,\text{syst}} \\ &\pm 0.0011_{\,\text{model}} . \end{aligned}$$

Charge correlation analysis:

$$\begin{aligned} \Delta^{e-\mu}_{b\to X\ell\nu} = -0.0015 &\pm 0.0021_{\,\text{stat}} \pm 0.0021_{\,\text{syst}} \\ &\pm 0.0004_{\,\text{model}} , \\ \Delta^{e-\mu}_{b\to c\to X\ell\nu} = -0.0009 &\pm 0.0031_{\,\text{stat}} \pm 0.0017_{\,\text{syst}} \\ &\pm 0.0005_{\,\text{model}} . \end{aligned}$$

The cuts applied on the b-tagging variable, on the jet-charge value and on the $p_\perp$ were also varied. The results, in both methods, were found to be stable.

8 Conclusions

Two different strategies have been adopted to distinguish the $b \to X\ell\nu$ and the $b \to c \to X\ell\nu$ decays in order to measure the inclusive semileptonic branching fractions of b hadrons, $BR(b \to X\ell\nu)$ and $BR(b \to c \to X\ell\nu)$. One measurement, based on the analysis of the lepton transverse momentum, is significantly affected by the uncertainty from the modelling of the $b \to X\ell\nu$ $p_\perp$ spectrum. The other is based on the charge correlation between the lepton and a charge estimator in the opposite hemisphere. This has smaller dependence on the modelling of the decay kinematics, but the determination of the $b \to X\ell\nu$ branching fraction suffers from the uncertainty on the rate of $b \to W \to \bar{c} \to \ell$ decays. In both cases the modelling of the inclusive $b \to X\ell\nu$ decay kinematics is based on the measured rates of the different c hadrons in the final state.

The values of $BR(b \to X\ell\nu)$ and $BR(b \to c \to X\ell\nu)$ measured with the two methods are consistent within errors and they have been averaged. The resulting values are

$$\begin{aligned}\mathrm{BR}(\mathrm{b}\to\mathrm{X}\ell\nu) &= 0.1070 \pm 0.0010_{\,\mathrm{stat}} \\ &\quad \pm 0.0023_{\,\mathrm{syst}} \pm 0.0026_{\,\mathrm{model}}\ , \\ \mathrm{BR}(\mathrm{b}\to\mathrm{c}\to\mathrm{X}\ell\nu) &= 0.0818 \pm 0.0015_{\,\mathrm{stat}} \\ &\quad \pm 0.0022_{\,\mathrm{syst}}\ {}^{+0.0010}_{-0.0014\,\mathrm{model}}\ ,\end{aligned}$$

in agreement with the latest measurements performed by other LEP experiments [23–26], and with the latest values from experiments running at the $\Upsilon(4S)$ resonance [19].

Acknowledgements. We wish to thank our colleagues from the accelerator divisions for the successful operation of LEP. It is also a pleasure to thank the technical personnel of the collaborating institutions for their support in constructing and maintaining the ALEPH experiment. Those of us from non-member states thank CERN for its hospitality.

References

1. A.H. Hoang, Z. Ligeti, A.V. Manohar, Phys. Rev. Lett.**82**, 277 (1999). Phys. Rev. D **59**, 074017 (1999)
2. I.I. Bigi, M. Shifman, N. Uraltsev, Ann. Rev. Nucl. Part. Sci. **47**, 591 (1997)
3. The Particle Data Group, Review of Particle Physics, Eur. Phys. J. C **3**, 1 (1998)
4. E. Bagan, P. Ball, V.M. Braun, P. Gosdzinsky, Nucl. Phys. B **432**, 3 (1994). Nucl. Phys. Lett. B **342**, 362 (1995). Nucl. Phys. Lett. B **351**, 546 (1995)
5. M. Neubert, C.T. Sachrajda, Nucl. Phys. B **483**, 339 (1997)
6. The ALEPH Collaboration, Study of the fragmentation of b quarks into B mesons at the Z peak, Phys. Lett. B **512**, 30 (2001)
7. The ALEPH Collaboration, ALEPH: a detector for electron-positron annihilations at LEP, Nucl. Instrum. Meth. A **294**, 121 (1990); B. Mours et al., The design, construction and performance of the ALEPH silicon vertex detector, Nucl. Instrum. Meth. A **379**, 101 (1996)
8. The ALEPH Collaboration, Performance of the ALEPH detector at LEP, Nucl. Instrum. Meth. A **360**, 481 (1995)
9. The ALEPH Collaboration, A measurement of R_b using a lifetime mass tag, Phys. Lett. B **401**, 150 (1997)
10. The ALEPH Collaboration, Heavy quark tagging with leptons in the ALEPH detector, Nucl. Instrum. Meth. A **346**, 461 (1994)
11. The ALEPH Collaboration, Update of electroweak parameters from Z decays, Z. Phys. C **60**, 71 (1993)
12. L. Lyons, D. Gibaut, P. Clifford, Nucl. Instrum. Meth. A **270**, 110 (1988)
13. The LEP Collaborations, ALEPH, DELPHI, L3 and OPAL, the LEP Electroweak Working Group, and the SLD Heavy Flavour and Electroweak Groups, A Combination of Preliminary Electroweak Measurements and Constraints on the Standard Model, CERN-EP/2001-021
14. The ALEPH, DELPHI, L3, OPAL Collaborations, the LEP Electroweak Working Group and the SLD Electroweak and Heavy Flavour Groups, Precision Electroweak Measurements on the Z resonance. Physics Report in preparation
15. The ALEPH, CDF, DELPHI, L3, OPAL and SLD Collaborations, Combined results on b-hadron production rates, lifetimes, oscillations and semileptonic decays, SLAC-PUB/8492, CERN-EP/2000-096
16. C. Peterson, D. Schlatter, I. Schmitt, P.M. Zerwas, Phys. Rev. D **27**, 105 (1983)
17. The LEP Collaborations, ALEPH, DELPHI, L3 and OPAL, Combining Heavy Flavour Electroweak Measurements at LEP, Nucl. Instrum. Meth. A **378**, 101 (1996)
18. J. G. Korner et al., Z. Phys. C **38**, 511 (1988). Z. Phys. C **41**, 690 (1989)
19. The Particle Data Group, Review of Particle Physics, Eur. Phys. J. C **15**, 1 (2000)
20. The DELCO Collaboration, The semileptonic decays of the D meson, Phys. Rev. Lett. **43**, 1073 (1979)
21. The MARK III Collaboration, A direct measurement of charmed D^+ and D^0 semileptonic branching ratios, Phys. Rev. Lett. **54**, 1976 (1985)
22. The CLEO Collaboration, Measurements of semileptonic branching fractions of B mesons at the Upsilon (4S) resonance, Phys. Rev. Lett. D **45**, 2212 (1992)
23. The OPAL Collaboration, Measurement of inclusive semileptonic branching fractions of b hadrons in Z^0 decays, Eur. Phys. J. C **13**, 225 (2000)
24. The L3 Collaboration, Measurement of R_b and $\mathrm{BR}(\mathrm{b}\to\mathrm{X}\ell\nu)$ at LEP using Double-Tag Methods, Eur. Phys. J. C **13**, 47 (2000)
25. The L3 Collaboration, Measurement of branching ratios $\mathrm{b}\to e\nu\mathrm{X}$, $\mu\nu\mathrm{X}$, $\tau\nu\mathrm{X}$ and $\nu\mathrm{X}$, Z. Phys. C **71**, 379 (1996)
26. The DELPHI Collaboration, Measurement of the semileptonic b branching fractions and average b mixing parameter in Z decays, CERN-EP/2000-157, to be published in Eur. Phys. J. C